ACS Sustainable Chemistry & Engineering

Research Article

pubs.acs.org/journal/ascecg

Cytotoxicity of ZnO Nanoparticles Can Be Tailored by Modifying Their Surface Structure: A Green Chemistry Approach for Safer Nanomaterials

Alex Punnoose,*[,†] Kelsey Dodge,[†] John W. Rasmussen,[‡] Jordan Chess,[†] Denise Wingett,[‡] and Catherine Anders[†]

[†]Department of Physics, Boise State University, Boise, Idaho 83725, United States

[‡]Department of Biological Science, Boise State University, Boise, Idaho 83725, United States

ABSTRACT: ZnO nanoparticles (NP) are extensively used in numerous nanotechnology applications; however, they also happen to be one of the most toxic nanomaterials. This raises significant environmental and health concerns and calls for the need to develop new synthetic approaches to produce safer ZnO NP, while preserving their attractive optical, electronic, and structural properties. In this work, we demonstrate that the cytotoxicity of ZnO NP can be tailored by modifying their surface-bound chemical groups, while maintaining the core ZnO structure and related properties. Two equally sized (9.26 ± 0.11 nm) ZnO NP samples were synthesized from the same zinc acetate precursor using a forced hydrolysis process, and their surface chemical structures were modified by using different reaction solvents. X-ray diffraction and optical studies showed that the lattice parameters, optical properties, and band gap (3.44 eV) of the two ZnO NP samples were similar. However, FTIR spectroscopy showed significant differences in the surface structures and surface-bound chemical groups. This led to major differences in the zeta potential, hydrodynamic size, photocatalytic rate constant, and more importantly, their cytotoxic effects on Hut-78 cancer cells. The ZnO NP sample with the higher zeta potential and catalytic activity displayed a 1.5-fold stronger cytotoxic effect on cancer cells. These results suggest that by modifying the synthesis parameters/conditions and the surface chemical structures of the nanocrystals, their surface charge density, catalytic activity, and cytotoxicity can be tailored. This provides a green chemistry approach to produce safer ZnO NP.

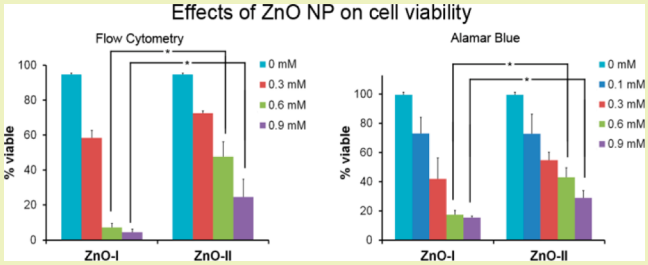

KEYWORDS: *Nanoparticles, Sustainability, Green chemistry, Oxides, Cancer, Cytotoxicity, Semiconductors*

INTRODUCTION

ZnO has many attractive optical properties including a high transparency, large exciton binding energy of 60 meV, and crystal structure very similar to GaN, making it a potential material for next generation optical and electronic applications such as UV laser diodes/LEDs, field effect transistors, gas sensors, solar cells, photodetectors, and peizoelectric generators.[1] Moreover, the superior catalytic activity of ZnO NP to generate hydrogen by the photolysis of water, photocatalytic degradation of water pollutants, decomposition of organic molecules[2,3] and certain organisms,[4,5] photoreduction of halogenated benzene derivatives and toxic metal ions, use in self-cleaning surfaces, and ability to detect biological species[6,7] have extended their applications into environmental remediation and biomedical research. Being considered as a "generally recognized as safe (GRAS)" substance by the U.S. Food and Drug Administration, ZnO is also used as a common food additive and a component in sun screens and cosmetics. It is in this context that the recent reports of the high cytotoxic effects of ZnO nanoparticles (NP) to both prokaryotic and eukaryotic systems pose a grave concern.[4,8−19] ZnO NP are among the most toxic engineered nanomaterials, especially among oxide NP.[14,20−22]

The numerous reports of the unusually high cytotoxicity of ZnO NP and their widespread use in various applications cause significant environmental and health concerns. This calls for a detailed investigation to identify the specific material features and properties that contribute to their strong cytotoxic effects. This information will also help researchers design new synthetic approaches to produce safer ZnO NP with minimal cytotoxicity, while preserving their important physicochemical properties such as their favorable crystal structure (isostructural to GaN) and the wide band gap that makes them attractive for their widespread use in technological applications. Although significant progress on the fabrication of ZnO nanostructures and their efficient applications in various technological fields have been achieved and a multitude of studies reporting their cytotoxic effects to various biological systems have already been

Special Issue: Sustainable Nanotechnology 2013

Received: February 27, 2014
Revised: May 17, 2014
Published: May 19, 2014

reported, only a few studies have attempted to make safer ZnO NP by design. George et al.[19] have reported the development of safer ZnO NP prepared by using a flame spray pyrolysis process that showed significant reduction in their cytotoxicity by doping with Fe ions. The lower cytotoxicity of the Fe-doped ZnO NP was attributed to improved ZnO bond strength and reduced NP dissolution. Another group recently reported a safer-by-design concept that involved hermetic encapsulation of ZnO nanorods in a biologically inert, nanothin, amorphous SiO2 coating using a modified flame spray pyrolysis synthesis.[22,23] The SiO_2 coating provided a 3-fold reduction in their DNA damage, while preserving their optoelectronic properties. Both of these approaches involved the introduction of foreign metal or metal oxide components, and these methods were limited to NP synthesis in gas phase. In this work, we propose a new approach for producing safer ZnO NP using wet chemical methods, without the use of foreign metal ions or oxides. We demonstrate that the cytotoxicity of ZnO NP can be tailored by modifying their surface chemical structure by comparing the cytotoxicity, physicochemical properties, and crystal structure of two 9.26 ± 0.11 nm-sized ZnO NP samples, both prepared from the same zinc acetate precursor using a forced hydrolysis process in two different reaction media. Differences in the surface chemical structure of the two ZnO NP samples are evident from the differences in their zeta potential, hydrodynamic size, and photocatalytic activity, and their cytotoxicity to Hut-78 cancer cells. In spite of their differences in surface structure and related properties, NP maintained their important optoelectronic properties such as band gap, optical absorption, and crystal structure. In our earlier studies, ZnO NP have shown strong preferential cytotoxicity to cancer cells such as Hut-78 lymphoma T cells, while displaying more than an order of magnitude lesser toxicity to their corresponding healthy primary T cells. This prompted us to use Hut-78 cancer cells for investigating the effect of NP surface modification on cytotoxicity.

EXPERIMENTAL DETAILS

Synthesis and Characterization of ZnO NPs. Chemically synthesized ZnO nanoparticles samples were thoroughly characterized and investigated in detail using X-ray diffraction (XRD), zeta potential measurements, dynamic light scattering, FTIR spectroscopy, and UV–vis spectrophotometry. X-ray diffraction (XRD) spectra were recorded at room temperature on a Philips X'Pert X-ray diffractometer with a Cu Kα source (λ = 1.5418 Å) in Bragg–Brentano geometry. The loose powder samples were leveled in the sample holder to ensure a smooth surface and mounted on a fixed horizontal sample plane. Lattice parameters and crystal size were analyzed with Rietveld refinement using Materials Analysis Using Diffraction (MAUD) software, corrected for instrumental broadening.[24]

Room-temperature optical spectra in the ultraviolet and visible light wavelength ranges were collected using a CARY 5000 spectrophotometer fitted with an integrating sphere diffuse reflectance accessory. The spectrophotometer measures reflectance relative to a background scatterer, which was powdered $BaSO_4$. Zeta potentials of the powdered samples of ZnO NPs were measured in nanopure water as a function of pH with a Malvern Zetasizer NanoZS. The temperature was equilibrated to 25 °C, and the pH was varied in the 6–12 range using 1.0 N HCl and 1.0 N NaOH prior to collecting the data. At least eight data collections per run were performed on three separate aliquots of the ZnO suspension for each sample. The hydrodynamic size of the ZnO samples suspended in nanopure water at a mass concentration of 30 μg/mL were measured at physiological pH using the zetasizer unit employing dynamic light scattering. Fourier transform infrared (FTIR) spectra were measured using a Bruker Tensor 27 spectrometer.

Catalytic Studies. The catalytic activity of the nanoparticles was investigated by measuring their ability to destroy a model fluorescent dye such as Rhodamine B. The samples were prepared in a solution of the model dye and nanopure water at 10 μM. For measuring photocatalytic rate constant, this solution was placed in a Rayonet RPR-100 UV reactor equipped with 2537 Å UV lamps delivering approximately 3.2 mW/cm^2. Before beginning optical absorption measurements, the samples were equilibrated for approximately 15 min, after which an initial sample was taken from the mixture before the lamps were turned on and then every 30 min after illumination. Liquid samples extracted from the reactor were placed in a centrifuge at 12,100g for 60 s to separate nanoparticles from the solution. The supernatant was then transferred to a quartz cuvette. and optical absorbance was measured on a Cary-5000 UV–vis spectrophotometer. This process continues with a fresh aliquot of solution every half hour for 2.5 h or until no absorption peak is visible.

Cell Culture and Cytotoxicity Studies. For cell cytotoxicity assays, the Hut-78 lymphoma T cell line (ATCC, Rockville, MD) was cultured in RPMI 1640 media supplemented with 10% FBS and 2 mM of L-glutamine, 1.5 g/L of sodium bicarbonate, 4.5 g/L of glucose, 10 mM HEPES, and 1.0 mM sodium pyruvate. Cells were maintained in log phase at 37 °C and 5% CO_2 and seeded at 1×10^5 cells/well in 96-well plates. Cells were subsequently treated with freshly sonicated (15 min) NPs reconstituted in phosphate buffered saline (PBS). For example, for a 2 mg/mL ZnO NP stock solution, 3.2 mg of NP was resuspended in 1.58 mL of PBS and sonicated at 50 W for 15 min. Then working dilutions were prepared from the NP stock solution and added to 200 μL of cell suspensions in 96-well plates and cultured for 24 h. NP concentrations are reported in molar units, but they can be converted to μg/mL units as needed, e.g., 0.3 mM = 24 μg/mL, 1 mM = 80 μg/mL, and 5 mM = 400 μg/mL. After 24 h, the effects of NPs on cell viability was assessed using flow cytometry by dually staining T cells with a fluorescein isothiocyanate labeled anti-HLA ABC antibody and 50 μg/mL of propidium iodide (PI) to monitor losses in membrane integrity. Fluorescent CountBright counting beads (Invitrogen, Carlsbad, CA) were added to samples to enable determinations of absolute cell numbers, and changes in PI staining were used to quantify cell death. Nanoparticles were excluded from analysis based on absence of fluorescence signal and light forward scatter (FS) and side scatter (SSC) characteristics, and samples were analyzed with an EPICS XL flow cytometer (Beckman Coulter).

To confirm the observed cytotoxicity results on Hut-78 cancer cells, a second viability assay was also employed. This assay uses the fluorogenic redox indicator dye, Alamar Blue, which becomes fluorescent upon reduction by mitochondrial enzymes in metabolically active cells. Cell populations were seeded into 96-well plates at 1×10^5 cells/well, treated with NPs for 18 h, and 20 μL of Alamar Blue added to cultures for an additional 6 h. Changes in fluorescence were evaluated spectrophotometrically using excitation/emission at 530/590 nm.

Statistical Analyses. Statistical analyses were performed using SAS, Inc. software (Cary, NC; version 9.3). Cytotoxicity data (Figure 6) were analyzed using repeated measures ANOVA with posthoc false discovery rate comparisons and significance levels defined as $p < 0.05$ to determine statistical differences between the means. The natural log of viability was used as the outcome to meet analysis assumptions regarding equal variance. This analysis allows within-sample variation to be separated from between-sample variation. Nanoparticles and concentration were defined as fixed factors, while the cell stock for individual experiments was defined as the repeated factor.

EXPERIMENTAL RESULTS AND DISCUSSION

ZnO NP synthesis. Our earlier studies[10,25,26] on the cytotoxicity of ZnO NP to cancer cells were all conducted using high purity samples produced by a forced hydrolysis method, using Zn acetate dehydrate as precursor and employing diethylene glycol (DEG) as the solvent (called ZnO-I). The solution was held at 150 °C for 90 min, and the amount of nanopure water allowed excellent control of the

crystallite size of ZnO NP.[26] Once cooled to room temperature, the NPs were separated from solution via centrifugation and subsequent washings with ethanol. In this work, a second wet chemical method is used to synthesize another set of ZnO NP (identified as ZnO-II) that also employs the same zinc acetate dihydrate precursor and a similar chemical hydrolysis method but used denatured ethanol as the reaction solvent and a strong base LiOH to maintain appropriate pH. The solution was held at 80 °C for 90 min, cooled to room temperature, and aged with *n*-heptane for several hours. The NPs were removed from solution via centrifuge, followed by subsequent washings with nanopure water and/or ethanol. After washings, the ZnO NP were dried in an oven at 65 °C for at least 12 h to obtain dry powders. These two types of ZnO NP, called ZnO-I and ZnO-II samples, showed significant differences in their physical and chemical properties, as discussed below. A bulk ZnO sample was also used for comparison. All of the as-purchased bulk ZnO samples from multiple commercial sources had a small fraction of the material as <10 nm crystallites. Presence of this small fraction of nanocrystals in the bulk samples unknowingly caused them to show some of the properties of the ZnO NP, leading to conflicting results. To avoid this, the commercially acquired bulk ZnO was annealed in air at 800 °C for 3 h before using them as bulk ZnO control. Such annealing will sinter any nanocrystals in them and will convert them to bulk crystals, but the core ZnO crystal structure will not be impacted by this process.

X-ray Diffraction Analysis for Crystal Structure and Morphology. X-ray diffraction (XRD) studies were employed to investigate phase purity, structural properties, and crystallite size. XRD patterns of ZnO-I and ZnO-II NP are shown in Figure 1. XRD patterns displayed the wurtzite ZnO phase, with

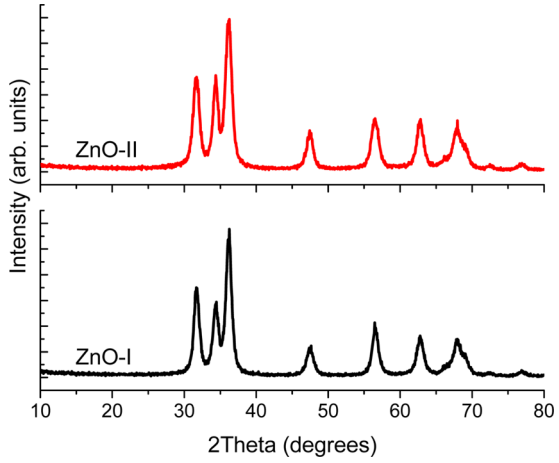

Figure 1. X-ray diffraction spectra of ZnO-I and ZnO-II NP.

no indication of any unwanted impurity phases. Rietveld refinement was used to calculate the lattice parameters *a* and *c* and lattice volume *V*. For the ZnO-I and ZnO-II samples, *a* values were 3.2582 and 3.2586 Å, *c* parameters were 5.2208 and 5. 2202 Å, and *V* values were 47.999 and 48.006 Å^3, respectively. The closeness of these lattice parameters for the two samples suggest that their core ZnO crystal structures are identical. Average crystallite sizes *L* of the ZnO NPs were calculated using the width of the peaks and the Scherrer relation, $L = 0.9\lambda/B \cos\theta$ (where θ is the peak position, λ is the X-ray wavelength, and peak width $B = (B_m^2 - B_s^2)^{1/2}$ was estimated using the measured peak width B_m and the instrumental width B_s). The average crystallite sizes of these two ZnO NP samples were also almost identical with 9.38 nm for ZnO-I and 9.15 nm for ZnO-II. Thus, the crystal structure and crystallite size of ZnO-I and ZnO-II are almost identical, and so if any differences in the physicochemical properties of these two samples are observed, those are most likely to be due to differences in the surface structure of the crystallites in these samples.

Surface Structure Studies Using FTIR Spectroscopy. Hydroxylation and presence of other surface-bound species on the ZnO NP can be investigated using Fourier transformed infrared (FTIR) spectroscopy. In order to unravel differences in the surface chemical structure of the ZnO NP, FTIR spectra of ZnO-I and ZnO-II NP were recorded and are shown in Figure 2. This data showed the expected strong characteristic Zn−O

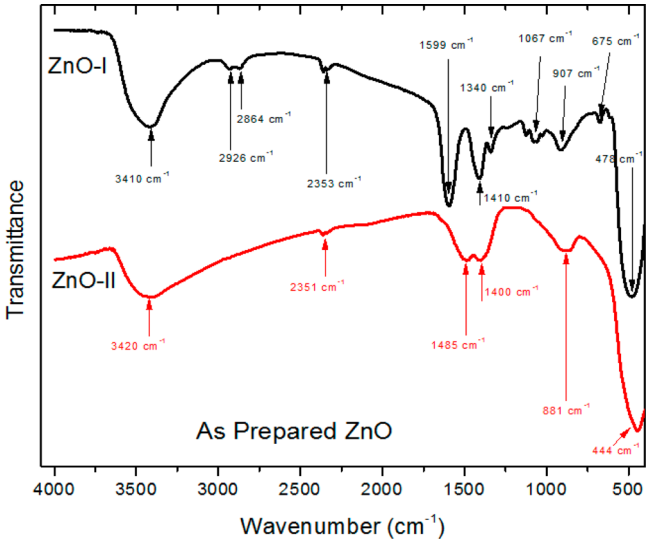

Figure 2. FTIR spectra of ZnO-I and ZnO-II NP, with the wave numbers of the main peaks marked.

vibrations[27] at 478 cm^{-1} in ZnO-I and 444 cm^{-1} in ZnO-II. Although the ZnO core structure on the two samples were almost identical as evident from similar lattice parameters, Zn−O bonds in the surface region of the NP are influenced by the surface-bound chemical groups, resulting in the difference of 34 cm^{-1} between them. The broad absorptions around 3410−3420 cm^{-1} due to hydroxyl groups attached on the nanoparticle surface are relatively stronger in ZnO-I. Studies have shown that the coordination of atoms on the surface of metal oxide nanostructures differ from that of their bulk/core, and coexistence of oxygen and metal-terminated layers have been observed.[28] Further stabilization occurred by chemical means in which charge reduction takes place by replacing oxygen at the surface by hydroxyl groups. The absorptions at 2926, 2864, 1340, and 1067 cm^{-1} indicate the presence of carbon-linked fragments of DEG on the surface of the ZnO-I NP, while these are absent in ZnO-II prepared in ethanol medium, a significant difference in the surface chemistry of the two types of ZnO NP. Absorption around 2351−2353 cm^{-1} is due to CO_2 molecules, which are present in both samples. The ZnO-I sample exhibits two strong bands, commonly associated with the carboxylate functional group, at 1412 cm^{-1} [ν_s(COO$^-$)] and 1595 cm^{-1} [ν_{as}(COO$^-$)].[29−32] Additionally, weaker bands consistent with τ(CH_2) and ν(C−OH) at 907 and 1067 cm^{-1}, respectively,

indicate the presence of surface-adsorbed groups possibly originating from the fragments of the acetate precursor and/or DEG.[30−33] ZnO-II NPs also showed many of these bands due to surface adsorbed groups resulting from the acetate groups but with somewhat lower intensity and at slightly different frequencies. Thus, these results clearly show that the surface structure and chemistry of the ZnO-I and ZnO-II NPs are significantly different, and this influences the surface layer of Zn−O bonds. This might influence the properties of ZnO NP that depend primarily on the surface structures.

Zeta Potential, Isoelectric Point, and Hydrodynamic Size. NP have large surface to volume ratios, and their surface consists of uncompensated dangling bonds and charged ions/groups. FTIR data has already shown that the surface structure of the two ZnO samples, ZnO-I and ZnO-II, prepared under different synthesis conditions/parameters are significantly different. This difference is expected to modify the net surface charge density and their interparticle interactions. When dispersed in an aqueous medium, nanocrystals undergo surface ionization and adsorption of ions, resulting in the generation of enhanced surface charge. This surface charge leads to an electric potential between the nanocrystals and the bulk of the dispersion medium, and this is measured as zeta potential in experiments that use electrophoretic/electrokinetic techniques. To obtain insight into the differences in the surface charge of the two ZnO NP samples, zeta potentials of the powdered samples suspended in nanopure water were measured. Figure 3

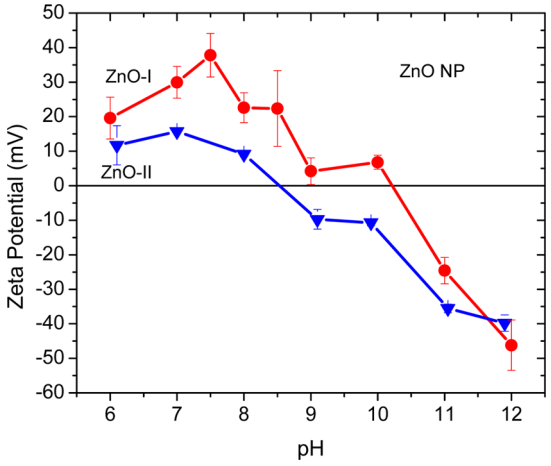

Figure 3. Zeta potentials of ZnO-I and ZnO-II NP measured as a function of pH.

shows plots of the zeta potentials of the ZnO-I and ZnO-II samples measured as a function of the solution pH. Zeta potential of ZnO-I NP sample was significantly higher than that of ZnO-II, as shown in Figure 3, and their values at the physiological pH of 7.5 were +42.6 mV and +12.5 mV, respectively. The isoelectric point (IEP) of the ZnO-I sample (~10) was significantly higher than that of ZnO-II NP (~8.5).

NPs of metal oxides (M_xO_y) such as ZnO usually have neutral hydroxyl groups attached to their surfaces, as evident from the FTIR data in Figure 2, forming M−OH surface layers, and this plays a crucial role in developing significant surface charge when prepared as nanocrystals. In aqueous medium and at higher pH values, the chemisorbed protons (H+) move out from the NP surface leaving a negatively charged surface with partially bonded oxygen atoms ($M-O^-$). At lower pH values, protons (H+) from the acidic solvent are transferred to the NP surface, developing positive charge due to the surface-bound $M-OH_2^+$ groups. The high isoelectric points (IEP) of ZnO NPs provide a strong positive surface charge/zeta potential at neutral and physiological pH ranges, and this might be one reason that they are easily attracted to the negatively charged cell membranes and display high cytotoxicity compared to many other oxides that have relatively lower IEPs.[34] The ZnO-I NP sample displayed a much higher zeta potential compared to the ZnO-II sample, and the former has a higher IEP value as well (Figure 3). Relative intensity of the FTIR peaks (Figure 2) of hydroxyl groups in the ZnO-I samples are much stronger compared to that of the ZnO-II samples, thus supporting the above hypothesis on the role of M−OH surface layers in the observed zeta potentials of ZnO NPs.[35]

Nanocrystals usually undergo agglomeration when dispersed in solutions, and this behavior has a major impact on the reactivity and response of nanomaterials upon exposure to various cells or organisms. Therefore, the hydrodynamic sizes of the ZnO samples suspended in nanopure water were measured at physological pH using dynamic light scattering. Interestingly, the hydrodynamic sizes of the ZnO NPs showed some correlation to their surface charges with the weakly positive ZnO-II samples forming an order of magnitude larger agglomerates (2386 ± 48 nm) compared to the more positively charged ZnO-I samples (623 ± 48 nm). According to the Derjaguin−Landau−Verwey−Overbeek (DLVO) model, agglomeration of uncapped nanocrystals depends on the repulsive interaction arising from electrostatic force and the van der Waals force of attraction. Because the surface charges of nanocrystals influence the electrostatic repulsive force, NP with larger zeta potential will generally reduce hydrodynamic size.

Optical Properties and Band Gap. Optical absorption studies were conducted using a UV−vis spectrophotometer (Figure 4), and both ZnO-I and ZnO-II samples showed a

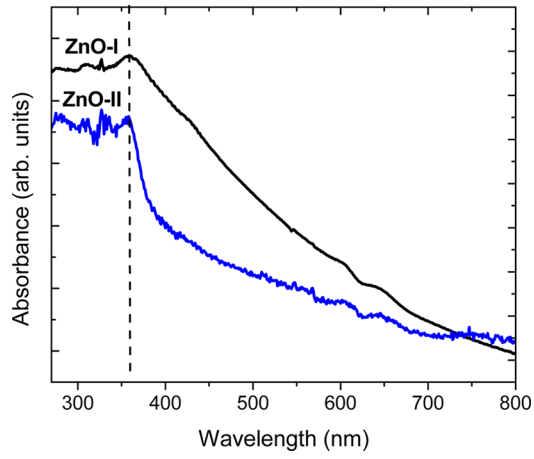

Figure 4. UV−visible spectra of ZnO-I and ZnO-II NP samples showing the band gap transition near 360 nm.

typical exciton absorption peak at 360 nm, which corresponds to a band gap energy of 3.44 eV. Bulk ZnO has a band gap of ~3.2 eV, which is in the near UV range. However, when prepared in nanoscale size, the band gap increases due to the quantum confinement effect, and this explains the larger band gap of the two ZnO NP samples. The band gap of semiconductor NPs has been proposed recently as a key

dx.doi.org/10.1021/sc500140x | ACS Sustainable Chem. Eng. 2014, 2, 1666−1673

parameter that determines their toxicological response at cellular and whole animal levels.[36]

Catalytic Activity and Rate Constant. It is widely believed that catalytic activity of oxide nanoparticles play a role in their cytotoxic response to biological systems, and so experiments were conducted to measure the catalytic rate constants of ZnO-I and ZnO-II NP.[22] Semiconductor materials can absorb any radiation with photon energy ($h\nu$) greater than the band gap energy E_B. Wide band gap oxides such as ZnO can absorb UV and other higher energy radiations, producing electron−hole pairs, and this has helped ZnO to act as one of the most promising photocatalysts.[37] The valence band holes (h^+) are powerful oxidants, and they can react with water or surface-bound chemisorbed hydroxyl groups producing hydroxyl ($OH^•$) radicals. Most organic photodegradation reactions utilize the oxidizing power of the holes directly or indirectly. The conduction band electrons (e^-) are good reductants and can move to the particle surface and get trapped in metastable surface states or react with electron acceptors or oxidants such as adsorbed O_2. Various activated reactive oxygen species (ROS) can be produced by the reactions of holes and/or electrons in a metal oxide semiconductor like ZnO with active sites. The active sites that make the semiconductor oxides efficient sensitizers for redox processes include surface-bound OH^- sites that are obviously abundant in large surface area ZnO-I and ZnO-II NP, as evident in the FTIR data (Figure 2).

The photocatalytic activity of the selected ZnO-I and ZnO-II nanoparticles were evaluated by comparing their ability to degrade a fluorescent model dye. In this work, Rhodamine B (RhB) was used as the model dye because it has a strong absorbance peak at 553 nm, allowing for monitoring its decomposition catalyzed by the NP. For photocatalytic degradation of the organic molecule RhB, each of the ZnO NP samples were first irradiated with UV light of wavelength 253.7 nm using a UV reactor delivering approximately 3.2 mW/cm^2.[37,38] Changes in the RhB absorbance peak intensity at different time points after treating with these UV irradiated ZnO NP samples were carefully measured using a spectrophotometer. The catalytic rate constant k for each ZnO NP sample was determined from the observed changes in the concentration of the dye in the solution. The photocatalytic rate constant k is given by

$$kt = \ln(C_0/C)$$

(where t = time, C_0 = initial concentration of RhB molecules, and C = concentration of the RhB molecules following its interaction with the nanoparticle sample for t seconds). The self-degradation of RhB under UV irradiation without the presence of ZnO nanoparticles was examined first and was found to be negligible. Adding UV irradiated bulk ZnO did not make a measurable effect in the RhB peak intensity. Interestingly, introduction of the UV-irradiated ZnO-I or ZnO-II NP to the RhB solution rapidly reduced the concentration of the organic dye as exposure time increased (Figure 5), thus clearly indicating the ability of ZnO NP to photocatalytically degrade the organic molecules. The photocatalytic rate constants k of the ZnO-I and ZnO-II NP samples were 0.128 and 0.0525 min^{-1}, respectively. Photocatalytic rate constants in the range of 0.005−0.055 min^{-1} have been reported for ZnO NP in the literature,[37,39] and these studies have shown that the exact value depends on the physicochemical properties of the NP such as size, shape, and morphology. The k value of ZnO-II is close to the highest k values reported

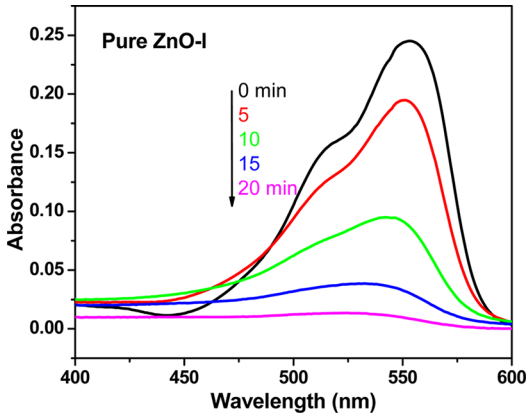

Figure 5. Plot showing the photocatalytic degradation of RhB dye in nanopure water treated with ZnO-I NP for different times indicated.

for ZnO NP in these studies, while the k value of the ZnO-I sample is about 2.5 times larger than that of the ZnO-II. This superior catalytic activity of both ZnO-I and ZnO-II NP samples may be due to the smaller size of 9.26 nm compared to 18−40 nm-sized ZnO NP used in those reports as well as differences in the surface structure, defect concentration, and morphology.[37,39] Compared to bulk or larger particles in which fast e^-—h^+ recombination hinders catalytic activity, the presence of temporary electron acceptors such as oxygen vacancies (and other surface defects) in small nanoparticles might help keep the e^-—h^+ pairs separate, preventing their tendency for fast recombination. These electrons and holes can reach the surface of NP more efficiently and participate in redox reactions to degrade organic molecules such as RhB.

In Vitro Cytotoxicity Studies. As mentioned earlier, cytotoxicity is a new property displayed by many materials, including ZnO, when prepared in the nanoscale size range. On the basis of our recent studies,[10] bulk ZnO did not show a measurable toxic effect, but ZnO NP displayed strong cytotoxicity to cancer cells such as Hut-78 lymphoma T cell lines. On the basis of this, we tried to investigate and compare the cytotoxicity of ZnO-I and ZnO-II NP to these cancer cells to determine if the differences in the surface structures and physicochemical properties of these two ZnO NP samples have a significant influence on their interaction with these cancer cells. Cells were maintained in log-growth phase at 37 °C and 5% CO_2. Cultures were then treated with each of the ZnO NP samples reconstituted in phosphate buffered saline (PBS). Efforts to obtain a stable NP stock solution included sonication for 10 min and immediately vortexing the stock solution before addition to cell cultures.

To assess the cell viability of the Hut-78 cancer cells treated with each of the ZnO NP samples, two different assays were employed: propidium iodide (PI) assay employing the flow cytometry system and Alamar blue assay reported in detail in our earlier papers.[4,10,12,25] For the PI-flow cytometry method, four different ZnO NP concentrations of 0, 0.3, 0.6, and 0.9 mM were employed, and the cell viability was determined after 24 h of treatment. The cell viability data of Hut-78 cells determined using the PI-flow cytometry method, shown in Figure 6A, confirm our previously reported strong cytotoxicity of ZnO NP to cancerous cells. It shows a rapid decrease in cell viability with increasing concentration of ZnO NP for both ZnO-I and ZnO-II samples. However, the ZnO-I NP sample showed a much faster reduction in the cell viability with

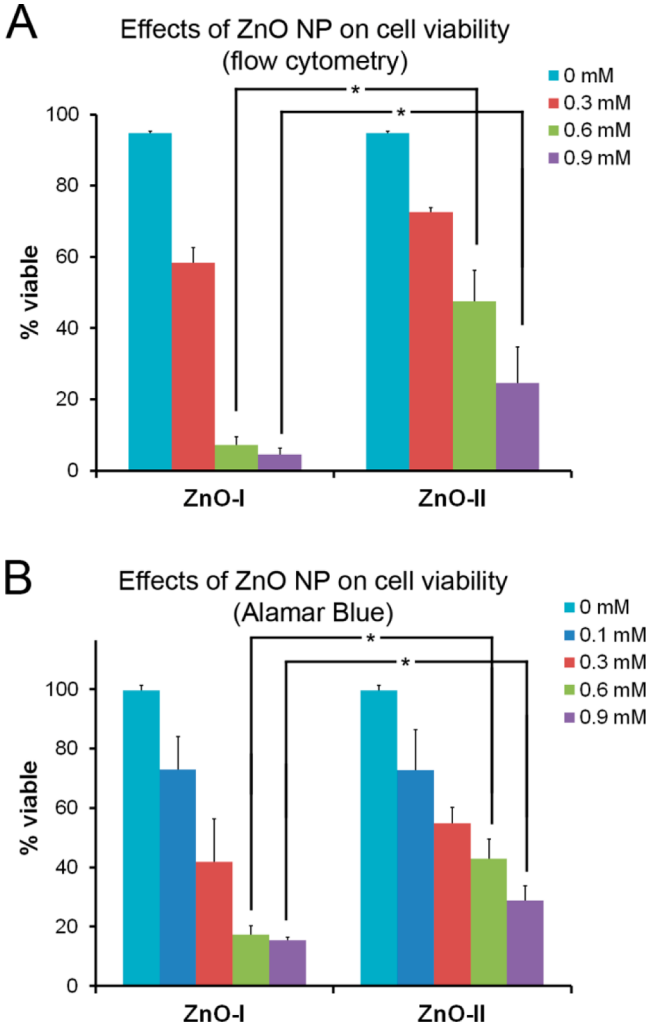

Figure 6. (A) and (B) display the cell viability of Hut-78 cancer cells after treating with ZnO-I and ZnO-II nanoparticles for 24 h at the concentrations indicated, determined using PI-flow cytometry and Alamar Blue methods, respectively. Bars represent the means ± standard error of three replicate experiments. *$p < 0.05$, significantly different from ZnO-I and ZnO-II.

increasing NP concentration compared to ZnO-II NP, so that the half maximal inhibitory concentration IC_{50} of ZnO-I was 0.37 mM while that of ZnO-II was 0.56 mM. Similar experiments using an independent Alamar blue assay (using five ZnO NP concentrations of 0, 0.1, 0.3, 0.6, and 0.9 mM) yielded a very similar trend but with slightly lower IC_{50} values of 0.31 mM for the ZnO-I samples as opposed to 0.45 mM for the ZnO-II NP sample (Figure 6b). Most importantly, in both assays, the ZnO-II NP samples showed about 1.5 times higher IC_{50} compared to that of the ZnO-I samples suggesting that ZnO-I NP samples are considerably more toxic than the ZnO-II samples.

ZnO-I and ZnO-II samples were prepared from the same precursor using a very similar forced hydrolysis process, and the primary difference was the use of DEG versus denatured ethanol as the reaction solvent. This is expected to only make differences in the surface structures/chemistry of the NP formed. This is further confirmed by the XRD and FTIR studies. XRD data analysis yielded almost identical crystallite size, ZnO crystal structures, and lattice parameters suggesting that the core ZnO structures of both ZnO-I and ZnO-II nanocrystals are identical. Similarly, optical data provided identical band gap energy for the two samples, which is another property of the core region of the nanocrystals. Because the primary differences observed between the ZnO-I and ZnO-II samples are in the surface chemical groups (from FTIR data), zeta potential that is related to the surface charge density, hydrodynamic size (which is also related to the ZP), and catalytic activity (and rate constant) that is very much a surface property, the significant difference observed in the cytotoxic response of the ZnO-I and ZnO-II samples to Hut-78 cells are attributed to these differences in their surface chemistry and surface-related properties. This result helps explain why the toxicity of ZnO NP formulations produced by different groups[10,11,17,21] differ so much. More importantly, it provides a new approach to tailor the cytotoxicity of ZnO NP by modifying their surface chemistry while maintaining their important properties such as band gap and optical absorption. More studies are necessary to improve this approach to eliminate the toxicity completely and to investigate the role of other material properties on the cytotoxic response of ZnO NP to cancer cells as well as to other cell types.

There have been reports[13,19] arguing that the ZnO NP toxicity results from dissolution of the NP into Zn^{2+} ions. We have earlier investigated this possibility by collecting the supernatant from the ZnO-I NP liquid stock. However, no appreciable toxicity was observed at the comparable volumes used for NP treatment.[25] Nevertheless, this may only indicate that any ZnO NP dissolution that may occur prior to cell entry at physiological pH is insufficient to account for the NP-induced cytotoxicity observed in our samples. More detailed studies to investigate nanoparticle uptake, intracellular localization, and potential extracellular and intracellular dissolution of nanoparticles will be pursued in the future to address this question.

CONCLUDING REMARKS

In conclusion, detailed investigations of equally sized ZnO nanocrystals prepared using two different wet chemical synthesis methods have shown that the cytotoxic response of ZnO NP samples to Hut-78 cancer cells depends on their surface structures and surface-related properties such as surface charge density, hydrodynamic size, and catalytic activity. This result also provides an understanding of why different formulations of equally sized ZnO NP exert different cytotoxic responses. The fact that all of these surface properties including cytotoxicity can be modified by tailoring the surface structures and chemistry provides a new approach to produce safer ZnO NP considering the widespread use of ZnO NP in nanotechnology applications.

AUTHOR INFORMATION

Corresponding Author

*E-mail: apunnoos@boisestate.edu.

Notes

The authors declare no competing financial interest.

ACKNOWLEDGMENTS

This work was supported in part by NSF CBET 1134468, NSF EAGER DMR-1137419, ARO W911NF-09-1-0051, and NIH 1R15CA141358 grants.

REFERENCES

(1) Hoye, R. L. Z.; Musselman, K. P.; MacManus-Driscoll, J. L. Research update: Doping ZnO and TiO_2 for solar cells. *APL Mater.* **2013**, *1*, 060701.

(2) Hoffmann, M. R.; Martin, S. T.; Choi, W.; Bahnemann, D. W. Environmental applications of semiconductor photocatalysis. *Chem. Rev.* **1995**, *95*, 69.

(3) Litter, M. I. Heterogenious photocatalysis − Transition metal ions in photocatalytic systems. *Applied Catalysis B: Environmental* **1999**, *23*, 89.

(4) Reddy, K. M.; Feris, K.; Bell, J.; Wingett, D. G.; Hanley, C.; Punnoose, A. Selective toxicity of zinc oxide nanoparticles to prokaryotic and eukaryotic systems. *Appl. Phys. Lett.* **2007**, *90*, 213902.

(5) Legrini, O.; Oliveros, E.; Braun, A. M. Photochemical processes for water treatment. *Chem. Rev.* **1993**, *93*, 671.

(6) Dorfman, A.; Kumar, N.; Hahm, J. I. Highly sensitive biomolecular fluorescence detection using nanoscale ZnO platforms. *Langmuir* **2006**, *22* (11), 4890−4895.

(7) Feris, K.; Pink, D.; Coombs, A.; Hanna, C. B.; Wingett, D.; Punnoose, A. Differential toxicity of ZnO nanoparticles to Pseudomonas aeruginosa bacterial strains with different membrane structure and charge. *Langmuir* **2008**, in preparation.

(8) Feris, K.; Otto, C.; Tinker, J.; Wingett, D.; Punnoose, A.; Thurber, A.; Kongara, M.; Sabetian, M.; Quinn, B.; Hanna, C.; Pink, D. Electrostatic interactions affect nanoparticle-mediated toxicity to the Gram-negative bacterium *Pseudomonas aeruginosa* PAO1. *Langmuir* **2010**, *26*, 4429−4436.

(9) Premanathan, M.; Karthikeyan, K.; Jeyasubramanian, K.; Manivannan, G. Selective toxicity of ZnO nanoparticles toward Gram-positive bacteria and cancer cells by apoptosis through lipid peroxidation. *Nanomedicine* **2011**, *7*, 184.

(10) Hanley, C.; Layne, J.; Punnoose, A.; Reddy, K. M.; Coombs, I.; Coombs, A.; Feris, K.; Wingett, D. Preferential killing of cancer cells and activated human T cells using zinc oxide nanoparticles. *Nanotechnology* **2008**, *19*, 295103.

(11) Taccola, V. R. L.; Riggio, C.; Vottorio, O.; Iorio, M. C.; Vanacore, R.; Pietrabiss, A.; Cischoeri, A. Zinc oxide nanoparticles as selective killers of proliferating cells. *Int. J. Nanomed.* **2011**, *6*, 1129.

(12) Hanley, C.; Thurber, A.; Hanna, C.; Punnoose, A.; Zhang, J.; Wingett, D. The influences of cell type and ZnO nanoparticle size on immune cell cytotoxicity and cytokine induction. *Nanoscale Res. Lett.* **2009**, *4*, 1409−1420.

(13) Xia, T.; Kovovich, M.; Liong, M. Comparison of the mechanism of toxicity of zinc oxide and cerium oxide nanoparticles based on dissolution and oxidative stress properties. *ACS Nano* **2008**, *2*, 2121.

(14) Sun, J.; Wang, S.; Zhao, D.; Hun, F. H.; Weng, L.; Liu, H. Cytotoxicity, permeability, and inflammation of metal oxide nanoparticles in human cardiac microvascular endothelial cells: Cytotoxicity, permeability, and inflammation of metal oxide nanoparticles. *Cell Biol. Toxicol.* **2011**, *27*, 333.

(15) Vandebriel, R. J.; De Jong, W. H. A review of mammalian toxicity of ZnO nanoparticles. *Nanotechnol. Sci. Appl.* **2012**, *5*, 61.

(16) De Angelis, I.; Barone, F.; Zijno, A.; Bizzarri, L.; Russo, M. T.; Pozzi, R.; FranchinI, F.; Giudetti, G.; Uboldi, C.; Ponti, J.; Rossi, F.; De Berardis, B. Comparative study of ZnO and TiO_2 nanoparticles: Physicochemical characterisation and toxicological effects on human colon carcinoma cells. *Nanotoxicology* **2013**, *8*, 1361.

(17) Bai, W.; Zhang, Z.; Tian, W.; He, X.; Ma, Y.; Zhao, Y.; Chai, Z. Toxicity of zinc oxide nanoparticles to zebrafish embryo: A physicochemical study of toxicity mechanism. *J. Nanopart. Res.* **2010**, *12*, 1645.

(18) Croteau, M. N.; Dybowska, A. D.; Luoma, S. N.; Valsami-Jones, E. A novel approach reveals that zinc oxide nanoparticles are bioavailable and toxic after dietary exposures. *Nanotoxicology* **2010**, *5*, 79.

(19) George, S.; Pokhrel, S.; Xia, T.; Gilbert, B.; Ji, Z.; Schowalter, M.; Rosenauer, A.; Damoiseaux, R.; Bradley, K. A.; Mdler, L.; Nel, A. E. Use of a rapid cytotoxicity screening approach to engineer a safer zinc oxide nanoparticle through iron doping. *ACS Nano* **2010**, *4* (1), 15−29.

(20) Kennedy, I. M.; Wilson, D.; Barakat, A. I. Uptake and inflammatory effects of nanoparticles in a human vascular endothelial cell line. *Res. Rep. - Health Eff. Inst.* **2009**, *136*, 3.

(21) Brunner, T. J.; Wick, P.; Manser, P.; Spohn, P.; Grass, R. N.; Limbach, L. K.; Bruinink, A.; Stark, W. J. In vitro cytotoxicity of oxide nanoparticles: Comparison to asbestos, silica, and the effect of particle solubility. *Environ. Sci. Technol.* **2006**, *40*, 4374.

(22) Sotiriou, G.; Watson, C.; Murdaugh, K.; Darrah, T. H.; Pyrgriotakis, G.; Elder, A.; Brain, J.; Demokritou, P. Engineering safer-by-design, transparent, silica-coated ZnO nanorods with reduced DNA damage potential. *Environ. Sci.* **2014**, *1*, 144−153.

(23) Gass, S.; Cohen, J. M.; Pyrgiotakis, G.; Sotiriou, G. A.; Pratsinis, S. E.; Demokritou, P. Safer formulation concept for flame-generated engineered nanomaterials. *ACS Sustainable Chem. Eng.* **2013**, *1*, 843−857.

(24) Lutterotti, L.; Scardi, P.; MaistrellI, P. LS1 − A computer-program for simultaneous refinement of material structure and microstructure. *J. Appl. Crystallogr.* **1992**, *25*, 459−462.

(25) Thurber, A.; Wingett, D. G.; Rasmussen, J. W.; Layne, J.; Johnson, L.; Tenne, D. A.; Zhang, J.; Hanna, C. B.; Punnoose, A. Improving the selective cancer killing ability of ZnO nanoparticles using Fe doping. *Nanotoxicology* **2012**, *6*, 440−452.

(26) Hanley, C.; Thurber, A.; Hanna, C.; Punnoose, A.; Zhang, J. H.; Wingett, D. G. The influences of cell type and ZnO nanoparticle size on immune cell cytotoxicity and cytokine induction. *Nanoscale Res. Lett.* **2009**, *4* (12), 1409−1420.

(27) Farbun, I. A.; Romanova, I. V.; Terikovskaya, T. E.; Dzanashvili, D. I.; Kirillov, S. A. Complex formation in the course of synthesis of zinc oxide from citrate solutions. *Russ. J. Appl. Chem.* **2007**, *80* (11), 1798−1803.

(28) Wang, X.-G.; Weiss, W.; Shaikhoutdinov, S. K.; Ritten, M.; Petersen, M.; Wagner, F.; Schlogl, R.; Scheffler, M. The hematite α-Fe_2O_3 (0001) surface: Evidence for domains of distinct chemistry. *Phys. Rev. Lett.* **1998**, *81*, 1038.

(29) Bian, S.-W.; Mudunkotuwa, I. A.; Rupasinghe, T.; Grassian, V. H. Aggregation and dissolution of 4 nm ZnO nanoparticles in aqueous environments: Influence of pH, ionic strength, size, and adsorption of humic acid. *Langmuir* **2011**, *27* (10), 6059−6068.

(30) Max, J. J.; Chapados, C. Infrared spectroscopy of aqueous carboxylic acids: Comparison between different acids and their salts. *J. Phys. Chem. A* **2004**, *108* (16), 3324−3337.

(31) Max, J. J.; Chapados, C. Infrared spectroscopy of aqueous carboxylic acids: Malic acid. *J. Phys. Chem. A* **2002**, *106* (27), 6452−6461.

(32) Rodriguez-Paez, J. E.; Caballero, A. C.; Villegas, M.; Moure, C.; Duran, P.; Fernandez, J. F. Controlled precipitation methods: Formation mechanism of ZnO nanoparticles. *J. Eur. Ceram. Soc.* **2001**, *21* (7), 925−930.

(33) Mudunkotuwa, I. A.; Rupasinghe, T.; Wu, C. M.; Grassian, V. H. Dissolution of ZnO nanoparticles at circumneutral pH: A study of size effects in the presence and absence of citric acid. *Langmuir* **2012**, *28* (1), 396−403.

(34) Chadwick, M. D.; Goodwinb, J. W.; Lawsonc, E. J.; Millsd, P. D. A.; Vincent, B. Surface charge properties of colloidal titanium dioxide in ethylene glycol and water. *Colloids Surf., A* **2002**, *203*, 229.

(35) Qu, F.; Morais, P. C. An oxide semiconductor nanoparticle in an aqueous medium: A surface charge density investigation. *J. Phys. Chem. B* **2000**, *104*, 5232.

(36) Zhang, H.; Ji, Z.; Xia, T.; Meng, H.; Low-Kam, C.; Liu, R.; Pokhrel, S.; Lin, S.; Wang, X.; Liao, Y.-P.; Wang, M.; Li, L.; Rallo, R.; Damoiseaux, R.; Telesca, D.; Mädler, L.; Cohen, Y.; Zink, J. I.; Nel, A. E. Use of metal oxide nanoparticle band gap to develop a predictive paradigm for oxidative stress and acute pulmonary inflammation. *ACS Nano* **2012**, *6*, 4349.

(37) Mclaren, A.; Valdes-Solis, T.; Li, G.; Tsang, S. C. Shape and size effects of ZnO nanocrystals on photocatalytic activity. *J. Am. Chem. Soc.* **2009**, *131*, 12540.

(38) Dodge, K.; Chess, J.; Eixenberger, J.; Alanko, G.; Hanna, C.; Punnoose, A. Role of oxygen defects on the magnetic properties of ultra-small $Sn_{1-x}Fe_xO_2$ nanoparticles. *J. Appl. Phys.* **2013**, *113*, 17B504.
(39) Gupta, J.; Barick, K. C.; Bahadur, D. Defect mediated photocatalytic activity in shape-controlled ZnO nanostructures. *J. Alloys Compd.* **2011**, *509*, 6725.